Schweizerischer Erdbebendienst
Service Sismologique Suisse
Servizio Sismico Svizzero
Swiss Seismological Service

ETH zürich

SITE CHARACTERIZATION REPORT

SVEJ: Vevey (VD) - Jardin du Rivage

Manuel Hobiger, Paolo Bergamo, Clotaire Michel, Donat Fäh

Last Modification: 8th December, 2017

Schweizerischer Erdbebendienst (SED)
Service Sismologique Suisse
Servizio Sismico Svizzero
Servizi da Terratrembels Svizzer

ETH Zürich
Sonneggstrasse 5
8092 Zürich
Schweiz
manuel.hobiger@sed.ethz.ch

Contents

1 Summary

The free-field strong-motion station SVEJ was built in the Jardin du Rivage in Vevey (VD). We performed a passive seismic array measurement to characterize the site. The measurements show that the fundamental frequency of the structure beneath the station is about 1.6 Hz.
The array measurements were analyzed with different techniques, namely 3-component HRFK, WaveDec and SPAC. All techniques gave similar dispersion curves. For Love waves, the dispersion curves for the fundamental and two higher modes were retrieved. For Rayleigh waves, the dispersion curves for the fundamental and one higher mode were identified. The measured ellipticity curves of different methods do not match with the H/V curves. Joint inversions of the dispersion curves and the H/V peak frequency yield velocity structures which consist of a smooth increase in S-wave velocity from 200 to 500 m/s in the superficial 30 m, followed by a first velocity contrast at 37 to 52 m of depth and a second velocity contrast with the seismic bedrock in depths between 100 and 150 m. The V_{S30} of the best models is about 351 m/s, corresponding to soil class C in both EC8 and SIA261.

2 Introduction

In the framework of the second phase of the Swiss Strong Motion Network (SSMNet) renewal project, a new station was planned to be installed in Vevey (VD). The Jardin du Rivage, close to Lake Geneva, was selected as the final location of the station. The new station, called SVEJ, went operational on 18 May 2016. The location of the station is shown in Fig. 1.

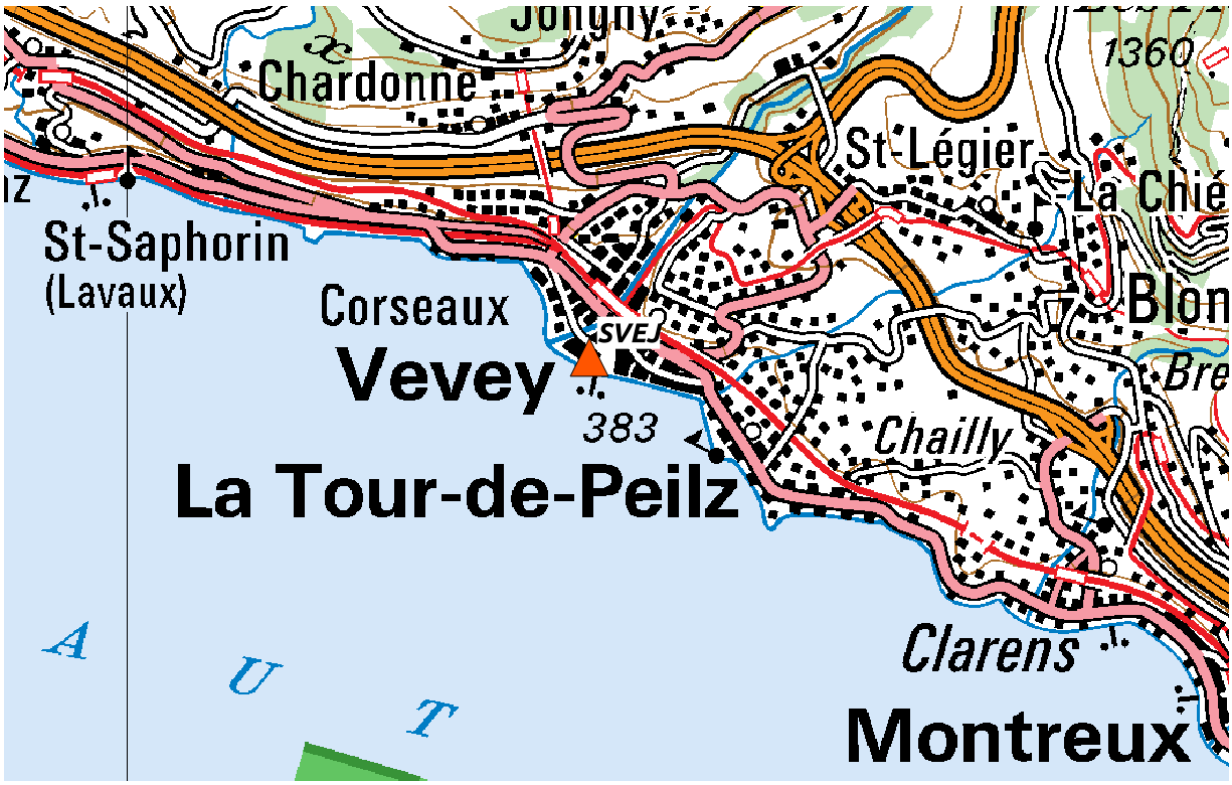

Figure 1: Map showing the location of station SVEJ in Vevey.

3 Geological setting

A geological map of the surroundings of station SVEJ is shown in Fig. 2. The station is located on the alluvial fan of the Veveyse river close to Lake Geneva. The center of Vevey is located on this alluvial fan, other parts of the town lie on a more complex geology built up by molasse, moraine, and quaternary deposits.
In the geological cadaster of the canton Vaud, we found the geological information of a borehole drilled in 1962 on the eastern side of the Grande Place, about 260 m east of the location of SVEJ. The geological profile is shown in Fig. 3. According to this profile, the alluvial deposits (gravels and sand) have a thickness of 49.5 m above the underlying molasse.

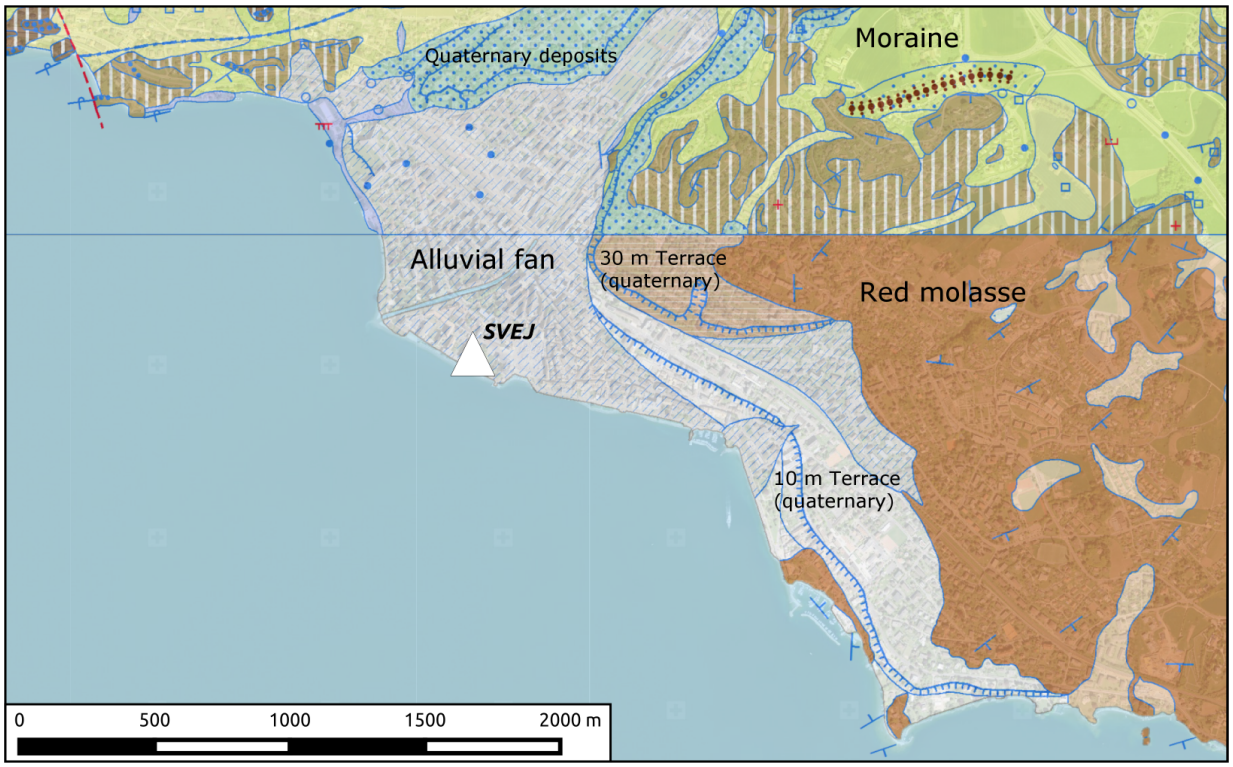

Figure 2: Geological map of the area around station SVEJ. According to the geological atlas, station SVEJ and all stations of the passive array measurement lie on alluvial deposits (grey area with blue dashes).

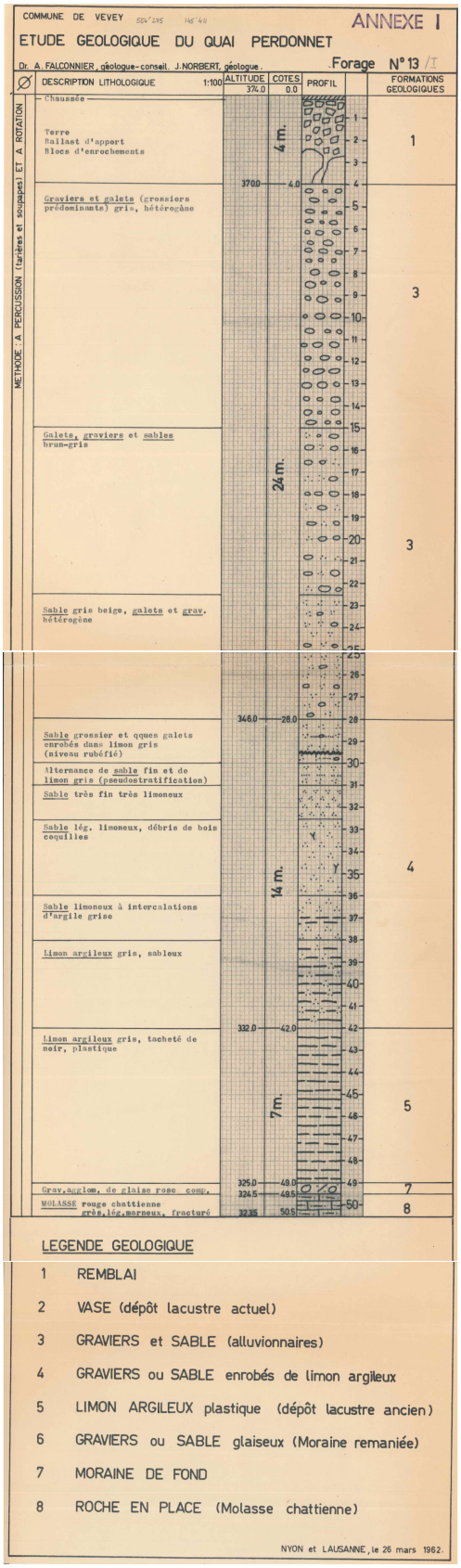

Figure 3: Geological profile from the eastern side of the Grande Place, about 260 m east of the location of SVEJ.

4 Site characterization

4.1 Measurements and data set

In order to characterize the local underground structure around station SVEJ, passive seismic array measurements were carried out on 23 November 2016. The layout of the seismic measurements is shown in Fig. 4.
A single large array of 16 stations was installed. The location close to the lake had to be taken into account for the array layout. The inner part of the array consisted of ten stations installed in the Jardin du Rivage. The stations were planned to be located on three rings of radii of 8, 20 and 50 m, respectively, around the central station. Three stations were installed on each ring with angular distances of 120°. One station on the eastern ring was placed directly east of the central station, the second ring was rotated by 25° clockwise with respect to the inner ring, the third ring was rotated by 20° clockwise with respect to the second ring. Six more stations were located further away in order to ensure a wide frequency range for the measurements.
Each installed station consisted of a Lennartz 5s sensor connected to a Centaur digitizer, where four stations in the central part had two sensors connected to the same digitizer. The station names of the array are composed of "SVEJ" followed by a two-digit number between 42 and 49, 52 and 55, 62, 66, 67 and 72 (corresponding to the Centaur digitizer serial number for numbers lower than 60 and serial number plus 20 for higher numbers). The minimum interstation distance in the array was 7.9 m, the maximum distance 451.2 m. The array recording time was 190 minutes (11400 s).
The station locations have been measured by a differential GPS system (Leica Viva GS10) which was set up to measure with a precision better than 5 cm. For most station locations, this precision was achieved. The precision for station SVEJ45 was 21.1 cm, for SVEJ47 9.0 cm and for SVEJ72 19.4 cm. At these locations, trees or high buildings altered the precision of the measurements.

Table 1: List of the passive seismic array measurements in Vevey.

Array name	Number of sensors	Minimum interstation distance [m]	Maximum interstation distance [m]	Recording time [s]
1	16	7.9	451.2	11400

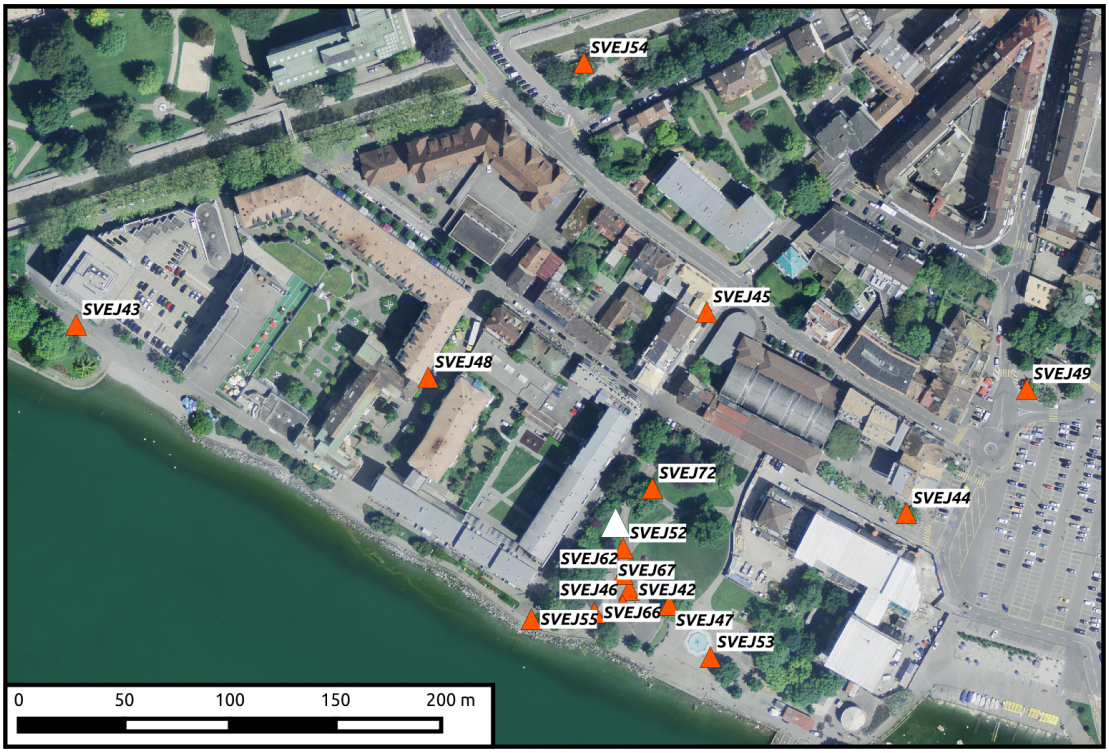

Figure 4: Layout of the array measurements around station SVEJ. The location of SVEJ is indicated by the white triangle, the locations of the stations for the passive seismic measurement by the orange triangles. ©2017 swisstopo (JD100042)

4.2 Measurement results

4.2.1 H/V curves

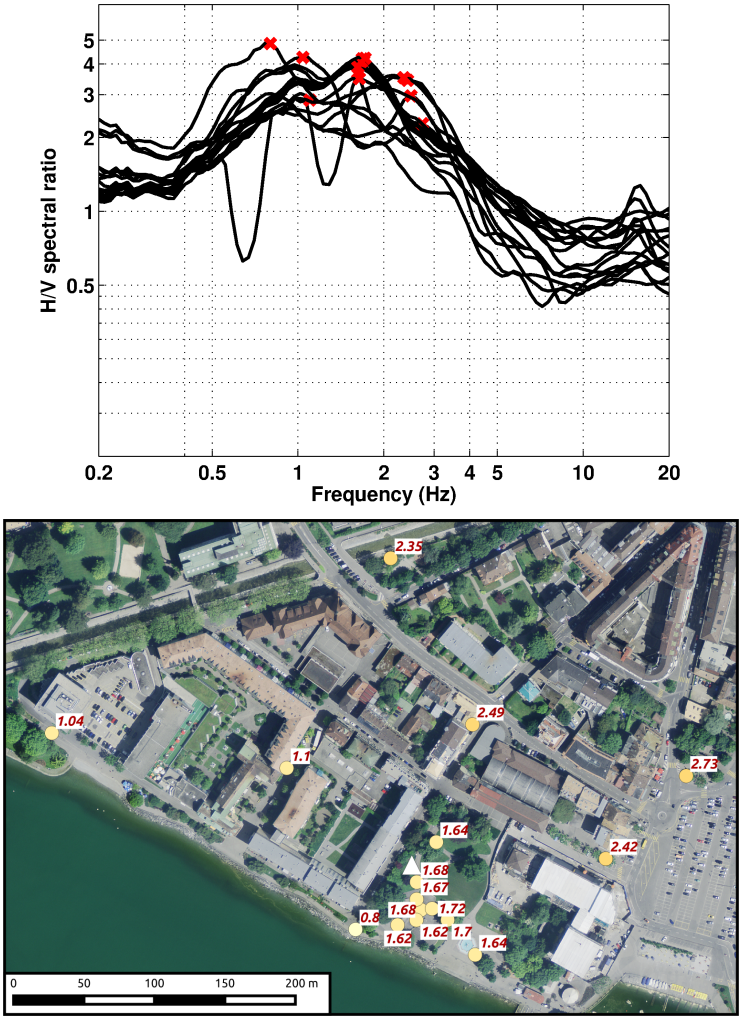

Figure 5: Overview of the H/V measurements for the different stations of the array measurement in Vevey.

Figure 5 shows the H/V curves determined with the time-frequency analysis method (Fäh et al., 2009) for all stations of the passive array and a map of the fundamental frequencies. The curves show a large degree of variability. All points in the Jardin du Rivage show a clear peak between 1.62 and 1.72 Hz. SVEJ55, located to the southwest in direct vicinity of the lake shore, shows a lower peak frequency of 0.8 Hz. This peak is partly visible at the other stations inside the Jardin du Rivage, but it is not the dominant peak there. Stations SVEJ43 and SVEJ48 show low resonance frequencies of around 1 Hz. The four stations located more to the north and northeast (SVEJ44, SVEJ45, SVEJ49 and SVEJ54) show higher resonance frequencies between 2.3 and 2.8 Hz, probably indicating a smaller sedimentary thickness in that area. Station SVEJ46 shows a strange H/V curve because there is a strong signal at 0.65 Hz and all of its multiples on the vertical component of the signal, causing local minima in the curve. The origin of this signal is unclear, the more as the stations around SVEJ46 do not show this behavior, although

they are only some meters away.
The H/V values at the peak frequency are relatively high and might be caused by a singularity of the Rayleigh wave ellipticity.

4.2.2 RayDec ellipticity curves

The RayDec technique (Hobiger et al., 2009) is meant to eliminate the contributions of other wave types than Rayleigh waves and give a better estimate of the ellipticity than the classical H/V technique. The RayDec ellipticity curves for all stations of the array measurements are shown in Fig. 6.
The RayDec curves also show quite a strong variability without well-marked peaks.

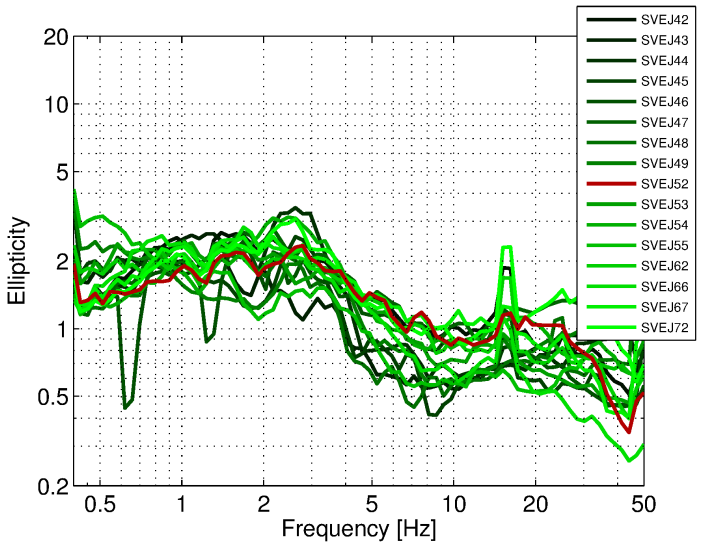

Figure 6: RayDec ellipticities for all stations of the array. The curve of SVEJ52, closest to the permanent station SVEJ, is highlighted in red.

4.2.3 Polarization measurements

The polarization analysis was performed according to Burjánek et al. (2010) and Burjánek et al. (2012). The results for all stations of the array are similar. Only the results for SVEJ52 are shown here.
There is no preferential linear particle polarization visible and also no preferential strike direction. We conclude that there are no 2-dimensional polarization effects.

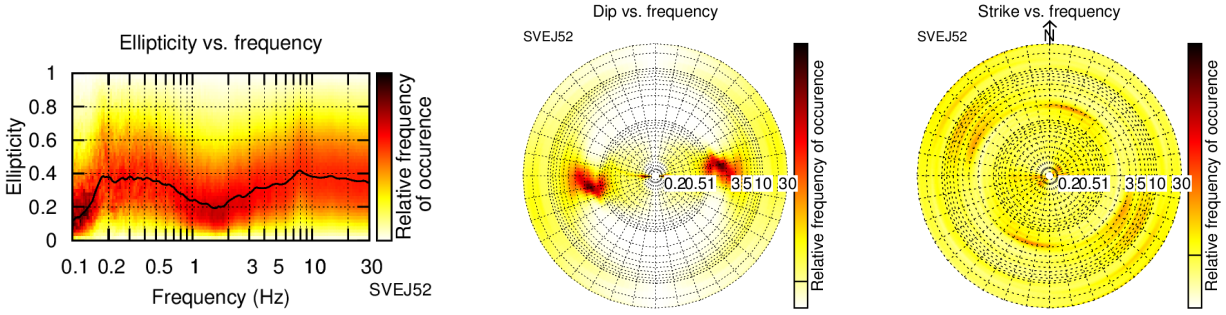

Figure 7: Polarization analysis of station SVEJ52.

4.2.4 3-component high-resolution FK

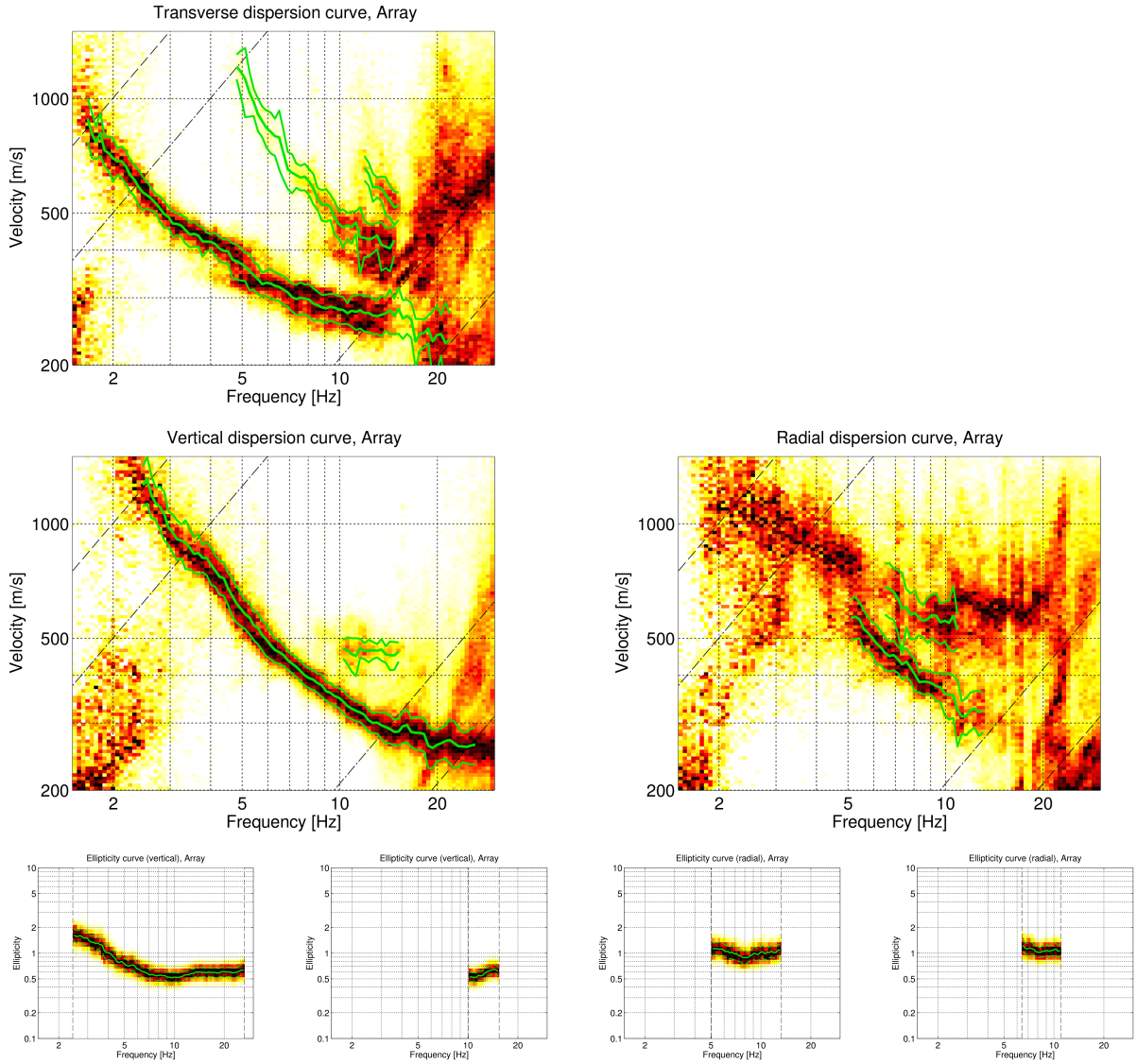

Figure 8: Dispersion and ellipticity curves obtained with the 3-component HRFK algorithm (Poggi and Fäh, 2010). The dispersion curves for the transverse, vertical and radial components are shown, as well as the ellipticity curves for the two modes picked on the vertical and the radial component. The dashed and dotted black lines are the array resolution limits. The solid green lines are picked from the data, where the central line indicates the best values and the two outer lines the standard deviation.

The results of the 3-component high-resolution FK analysis (Poggi and Fäh, 2010) are shown in Fig. 8. On the transverse component, the dispersion curve of the fundamental mode of Love waves is clearly visible in a wide range from below 2 to over 20 Hz. In addition, two higher modes can clearly be identified and picked.
On the vertical component, the fundamental mode of Rayleigh waves is visible between about 2.5 and 26 Hz. A small part of a harmonic mode is also visible. On the radial component, the fundamental mode can only partly be identified, but more higher modes are seen, but less clear than on the vertical and transverse components.
The corresponding ellipticity curves of the vertical and radial components can be clearly identified in the respective frequency ranges.

4.2.5 WaveDec

The results of the WaveDec (Maranò et al., 2012) processing are shown in Fig. 9. This technique estimates the properties of single or multiple waves simultaneously with a maximum likelihood approach. In order to get good results, the parameter γ has been tuned to modify the sharpness of the wave property estimation between purely maximum likelihood estimation and a Bayesian Information Criterion. Here, a value of $\gamma = 0.2$ was used, corresponding to a mainly maximum likelihood estimation.
The Love wave dispersion curve of the fundamental mode is clearly retrieved between 2 and 16 Hz. The Rayleigh wave dispersion curve of the fundamental mode is picked between 3 and 17 Hz. The ellipticity angle for the picked Rayleigh wave dispersion curve is positive below 5 Hz, indicating prograde particle motion, and negative above 5 Hz, indicating retrograde particle motion, but the change from one to the other is very abrupt. The ellipticity curve obtained by applying the *tan* function to the absolute value of the ellipticity angle does not show any clear peak or trough at 5 Hz. Anyhow, if we assume that the measured dispersion and ellipticity curves correspond to the fundamental mode of Rayleigh waves, the particle motion has to be retrograde at very low frequencies and there has to be a change from prograde to retrograde particle motion somewhere below 3 Hz, corresponding to a singularity in the ellipticity curve.

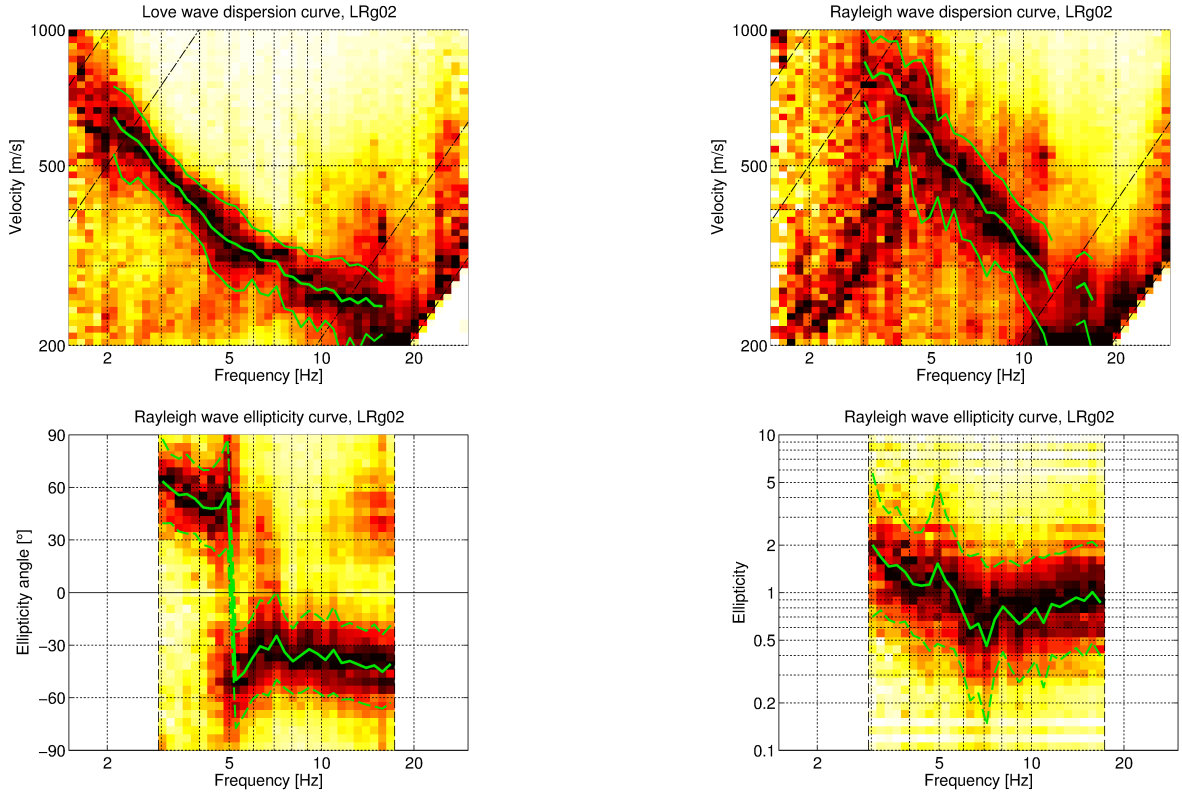

Figure 9: Love and Rayleigh wave dispersion (top) and ellipticity (bottom) curves obtained with the WaveDec technique (Maranò et al., 2012). The dashed lines indicate the theoretical array resolution limits.

4.2.6 SPAC

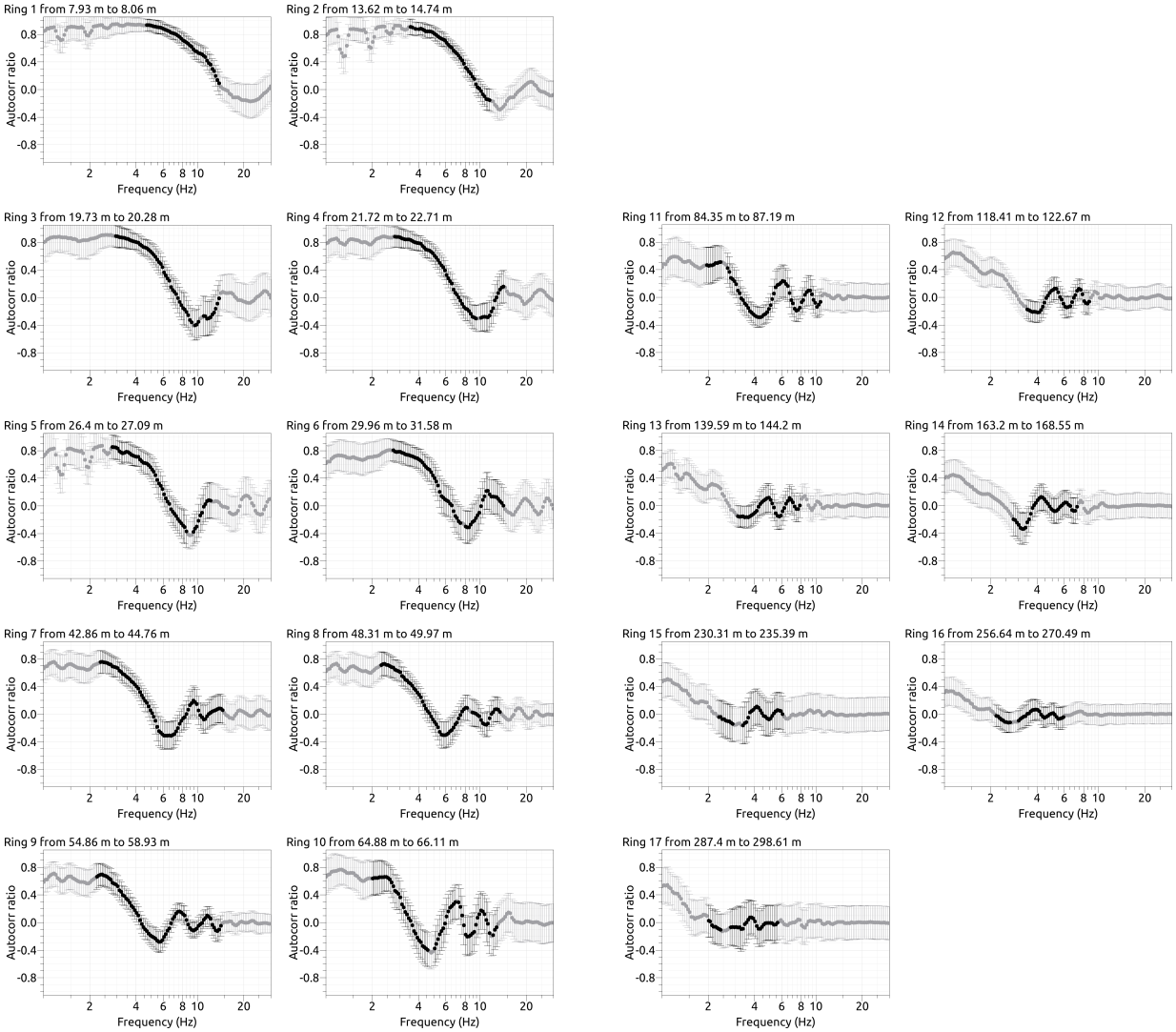

Figure 10: SPAC curves. The black data points contributed to the dispersion curve estimation.

The SPAC (Aki, 1957) curves of the vertical components have been calculated using the M-SPAC (Bettig et al., 2001) technique implemented in geopsy. Rings with different radius ranges had been defined previously and for all station pairs with distance inside this radius range, the cross-correlation was calculated in different frequency ranges. These cross-correlation curves are averaged for all station pairs of the respective ring and give the SPAC curves. The rings are defined in such a way that at least three station pairs contribute and that their connecting vectors have a good directional coverage.
The SPAC curves for all defined rings are shown in Fig. 10. The black points indicate the data values which contributed to the final dispersion curve estimation, which was made with the function `spac2disp` of the geopsy package. These resulting dispersion curves are shown in Fig. 11.
Using SPAC, we can pick a Rayleigh wave dispersion curve between 2.3 and 13.8 Hz.

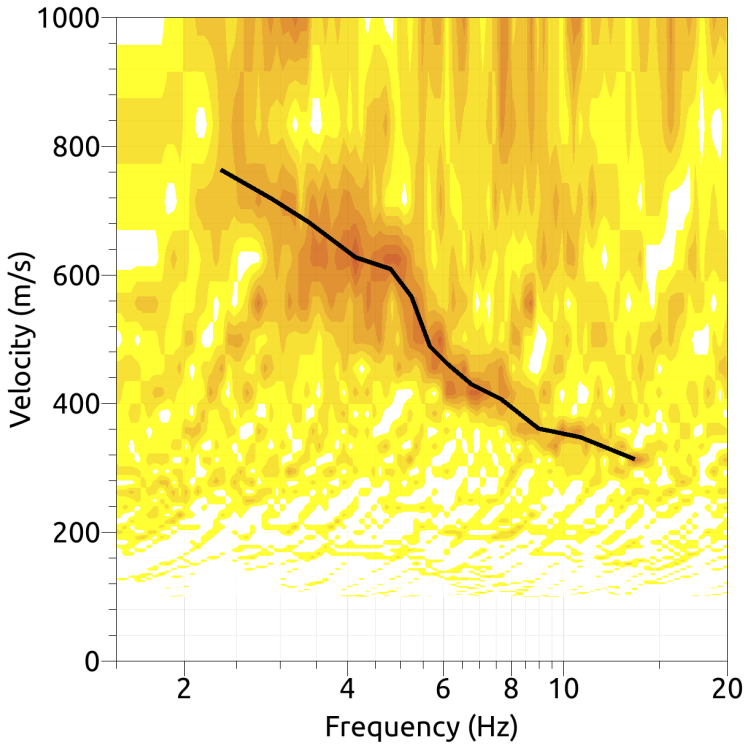

Figure 11: Resulting Rayleigh wave velocities. The black line corresponds to the picked dispersion curve.

4.3 Summary

Fig. 12 gives an overview of the dispersion and ellipticity curves determined by the different methods.
For Love waves, the HRFK and WaveDec results for the fundamental mode are in very good agreement, with slightly lower velocities determined by WaveDec. The two higher modes were identified for HRFK only.
For the Rayleigh waves, there is also a very good agreement between the different methods. The dispersion curve measured with SPAC shows lower velocities than the other methods below 5 Hz. The two parts of the higher modes obtained from the vertical and radial components using HRFK seem to belong to the same higher mode, but fit together only partly.
The ellipticity curves retrieved using the different methods are quite variable. The WaveDec curve lies between the RayDec and the HRFK curves, the HRFK curves of the higher modes are similar to the RayDec curves. WaveDec showed an abrupt change between retrograde and prograde particle motion at 5 Hz, but no singular peak or trough at that frequency. The H/V curves showed a fundamental frequency of around 1.7 Hz in the Jardin du Rivage, around the location of SVEJ. Such a resonance frequency seems lower than what the other methods show.

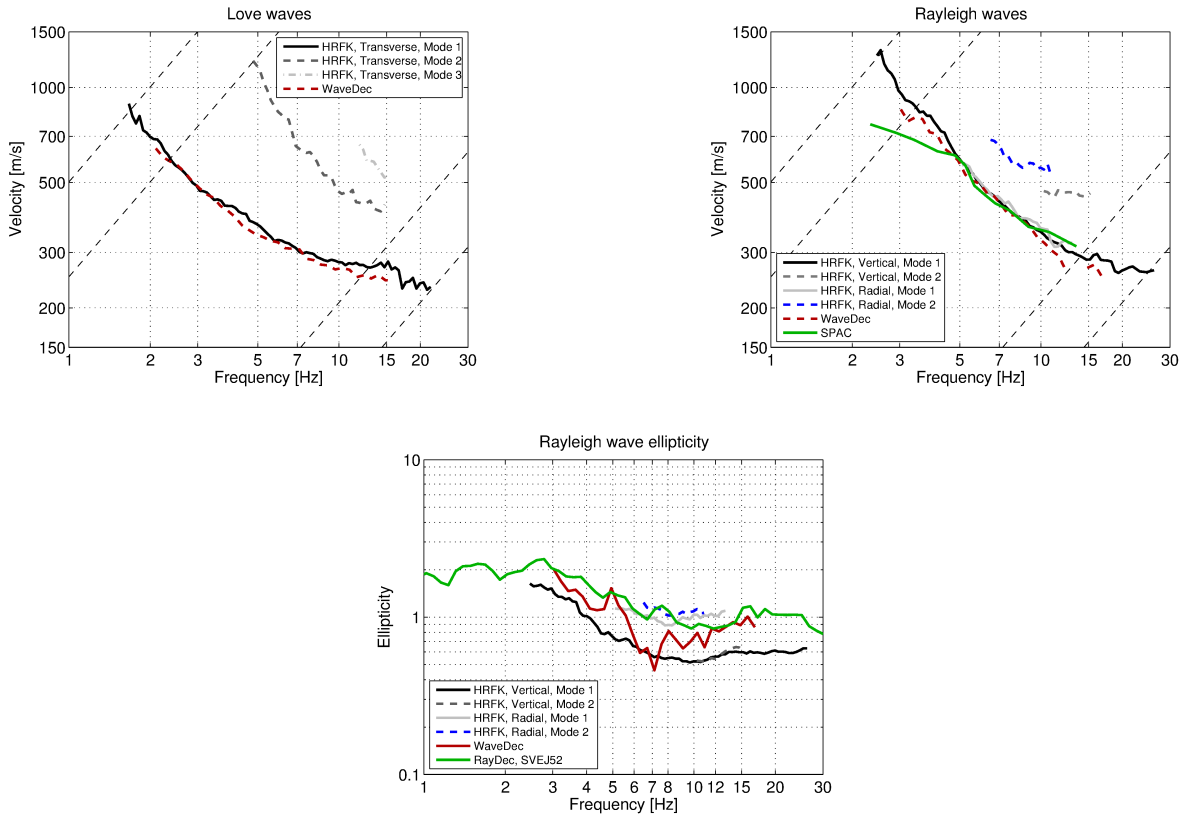

Figure 12: Overview of the Love and Rayleigh wave dispersion curves as well as the ellipticity curves for both arrays. The dashed lines indicate the theoretical resolution limits of the array. The RayDec ellipticity curve corresponds to station SVEJ43.

5 Data inversion

5.1 Inversion targets

We performed inversions using as much information as possible. The Rayleigh and Love wave dispersion curves measured with HRFK were assumed to correspond to the fundamental, first and second harmonic modes. The two parts of the higher mode detected with HRFK on the vertical and radial components were partly cut to fit together. We tried to use the RayDec ellipticity curve as an additional target, but without useful results. It was possible to fit the RayDec ellipticity curve, but then there was no singularity and no strong velocity contrast in the resulting profiles and also no resonance frequency between 1.6 and 1.7 Hz. Not constraining the resonance frequency at all resulted in velocity profiles with resonance frequencies of around 3 Hz, also not compatible with the measured resonance peak. Therefore, we used the fundamental frequency of $1.62 \pm .10\ Hz$ as an additional inversion target, without fixing if this peak is a singularity or not. The details of the inversion targets are indicated in Table 2 and the corresponding curves are shown in Fig. 13.

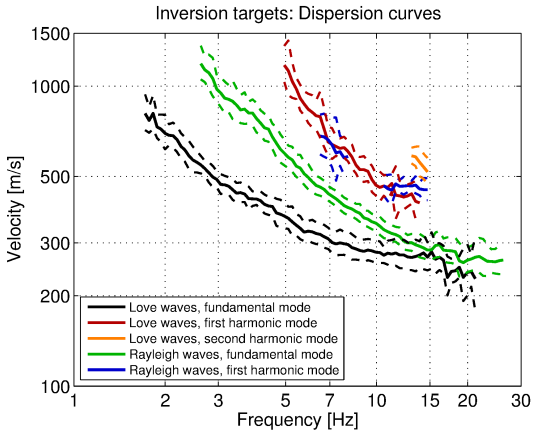

Figure 13: Overview of the dispersion curves used as targets for the different inversions.

Table 2: List of the data curves used as target in the inversion.

Method	Wave type	Mode	Curve type	Frequency range [Hz]
HRFK (T)	Love	fundamental	dispersion	1.7 - 21.2
HRFK (T)	Love	first higher	dispersion	4.9 - 14.0
HRFK (T)	Love	second higher	dispersion	13.0 - 15.0
HRFK (V)	Rayleigh	fundamental	dispersion	2.6 - 26.1
HRFK (V)	Rayleigh	first higher	dispersion	10.6 - 15.0
HRFK (R)	Rayleigh	first higher	dispersion	6.5 - 8.0
H/V	Rayleigh	fundamental	peak	1.62 ± 0.10 Hz

5.2 Inversion parameterization

For the inversion, seven different parameterizations have been used in total. The first six had free values of the depths and velocities of the different layers, ranging from three to eight layers (including half-space). The last parameterization had fixed layer depths and consisted of 17 layers in total, with the deepest interface at 150 m depth. S- and P-wave velocities were allowed to range from 50 to 3500 m/s and from 100 to 5000 m/s, respectively. The deepest layers were allowed to range to a depth of 200 m for the first six parameterizations. The density was fixed to 2 300 kg/m^3 for the lowest layer and to 2 000 kg/m^3 for all other layers.

5.3 Inversion results

We performed a total of seven inversions with different parameterizations (see Table 3). Each inversion run produced 200 000 total models in order to assure a good convergence of the solution. The results of these inversions are shown in Figs 14 - 20.
All inversions with more than three layers yielded very similar minimum misfit values and fit the data comparably well. The inversion using only three layers has a higher misfit, certainly because the model does not have enough complexity to explain the data. Using the fixed layer approach, the minimum misfit was slightly smaller than for the other inversions.

Table 3: List of inversions

Inversion	Number of layers	Number of models	Minimum misfit
SVEJ3l	3	200 000	0.602
SVEJ4l	4	200 000	0.420
SVEJ5l	5	200 000	0.445
SVEJ6l	6	200 000	0.415
SVEJ7l	7	200 000	0.432
SVEJ8l	8	200 000	0.431
SVEJfix	17	200 000	0.384

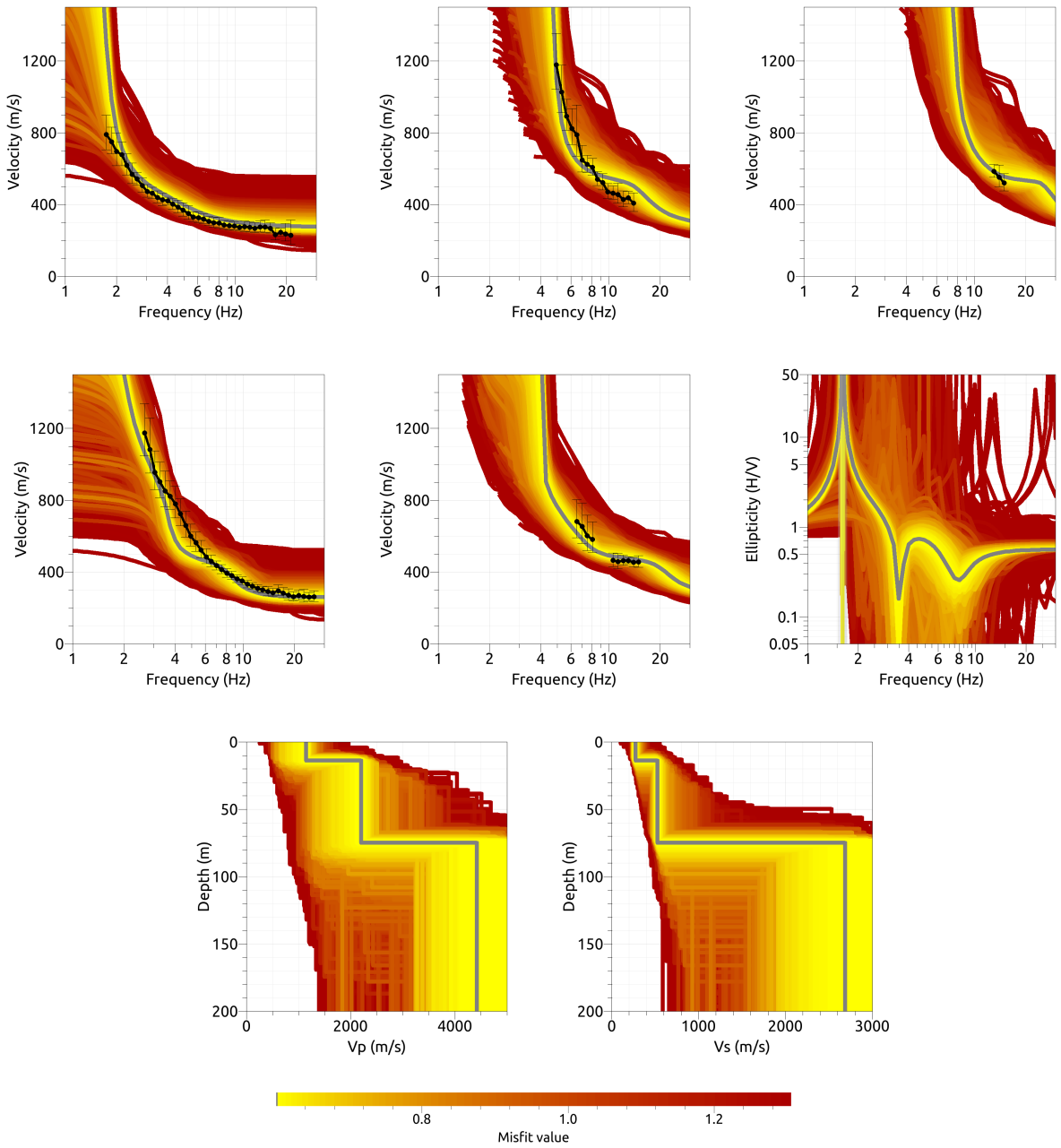

Figure 14: Inversion SVEJ3l. Top line: Dispersion curves for the Love wave fundamental mode (left), first harmonic mode (center) and second harmonic mode (right). Center line: Dispersion curves for the Rayleigh wave fundamental mode (left) and first harmonic mode (center), ellipticity curve of the Rayleigh wave fundamental mode (right). Bottom line: P-wave velocity profiles (left) and S-wave velocity profiles (right). The black dots indicate the data points used for the inversion, the gray line indicates the best-fitting model.

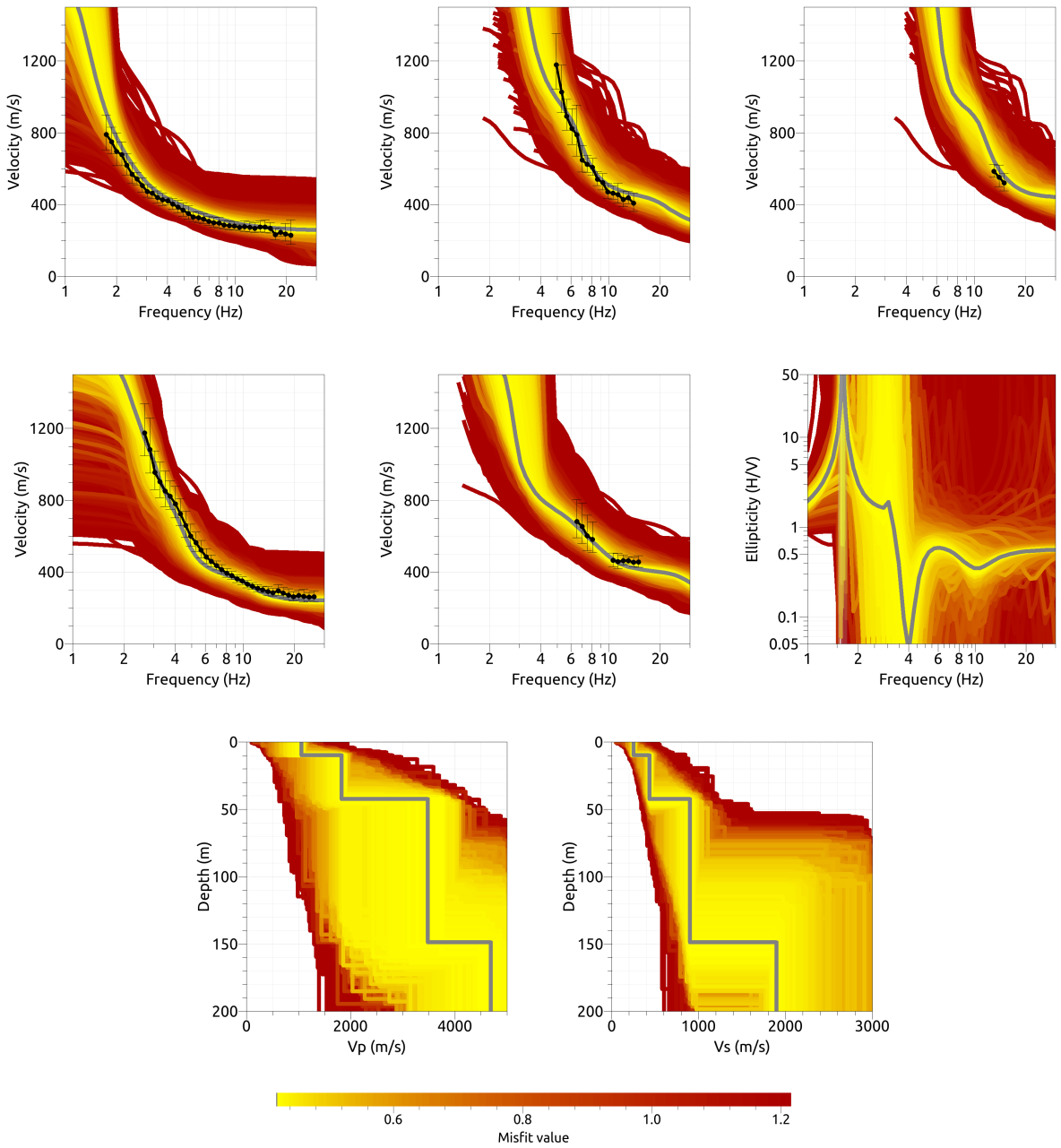

Figure 15: Inversion SVEJ4l. Top line: Dispersion curves for the Love wave fundamental mode (left), first harmonic mode (center) and second harmonic mode (right). Center line: Dispersion curves for the Rayleigh wave fundamental mode (left) and first harmonic mode (center), ellipticity curve of the Rayleigh wave fundamental mode (right). Bottom line: P-wave velocity profiles (left) and S-wave velocity profiles (right). The black dots indicate the data points used for the inversion, the gray line indicates the best-fitting model.

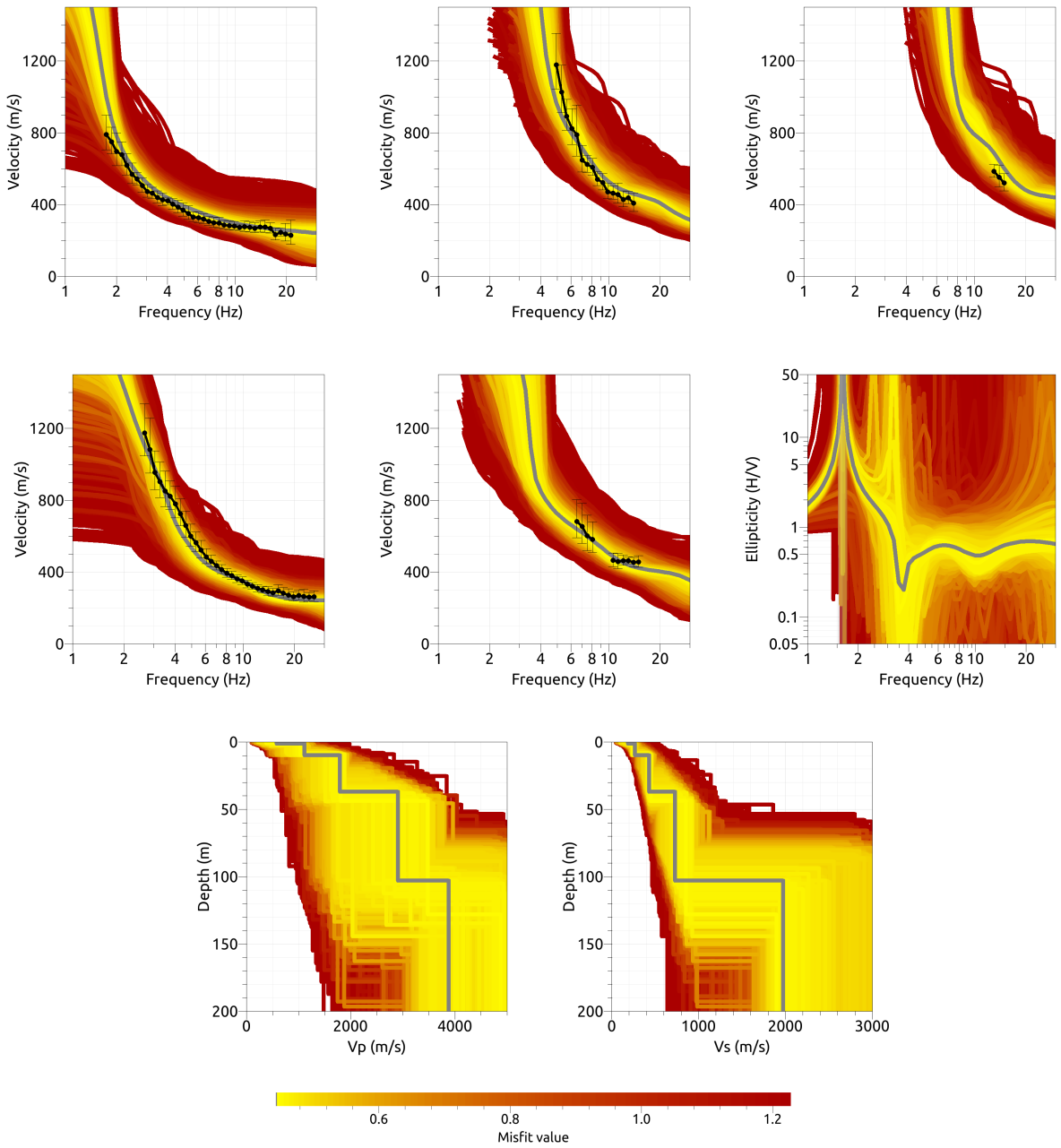

Figure 16: Inversion SVEJ5l. Top line: Dispersion curves for the Love wave fundamental mode (left), first harmonic mode (center) and second harmonic mode (right). Center line: Dispersion curves for the Rayleigh wave fundamental mode (left) and first harmonic mode (center), ellipticity curve of the Rayleigh wave fundamental mode (right). Bottom line: P-wave velocity profiles (left) and S-wave velocity profiles (right). The black dots indicate the data points used for the inversion, the gray line indicates the best-fitting model.

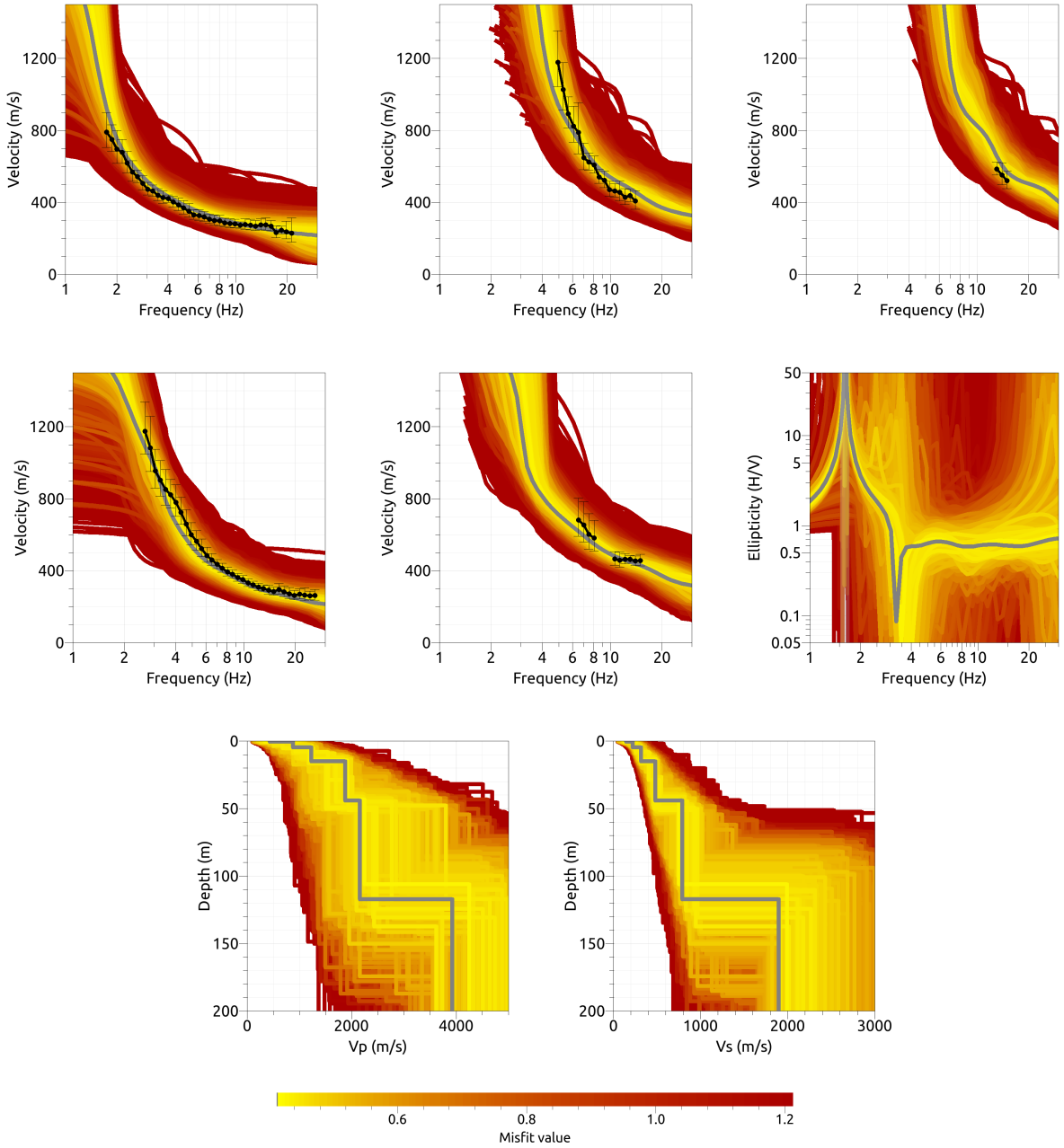

Figure 17: Inversion SVEJ6l. Top line: Dispersion curves for the Love wave fundamental mode (left), first harmonic mode (center) and second harmonic mode (right). Center line: Dispersion curves for the Rayleigh wave fundamental mode (left) and first harmonic mode (center), ellipticity curve of the Rayleigh wave fundamental mode (right). Bottom line: P-wave velocity profiles (left) and S-wave velocity profiles (right). The black dots indicate the data points used for the inversion, the gray line indicates the best-fitting model.

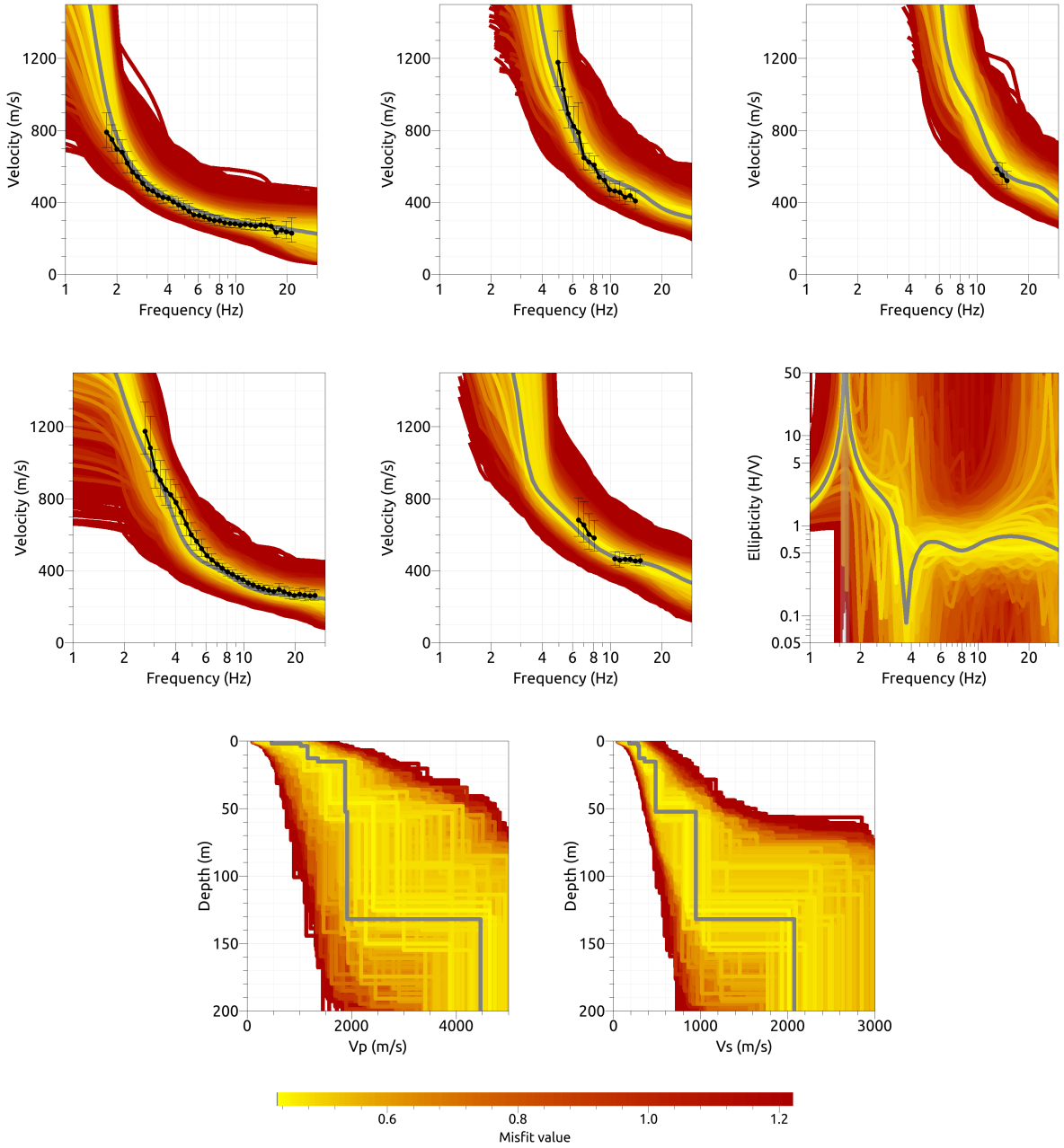

Figure 18: Inversion SVEJ7l. Top line: Dispersion curves for the Love wave fundamental mode (left), first harmonic mode (center) and second harmonic mode (right). Center line: Dispersion curves for the Rayleigh wave fundamental mode (left) and first harmonic mode (center), ellipticity curve of the Rayleigh wave fundamental mode (right). Bottom line: P-wave velocity profiles (left) and S-wave velocity profiles (right). The black dots indicate the data points used for the inversion, the gray line indicates the best-fitting model.

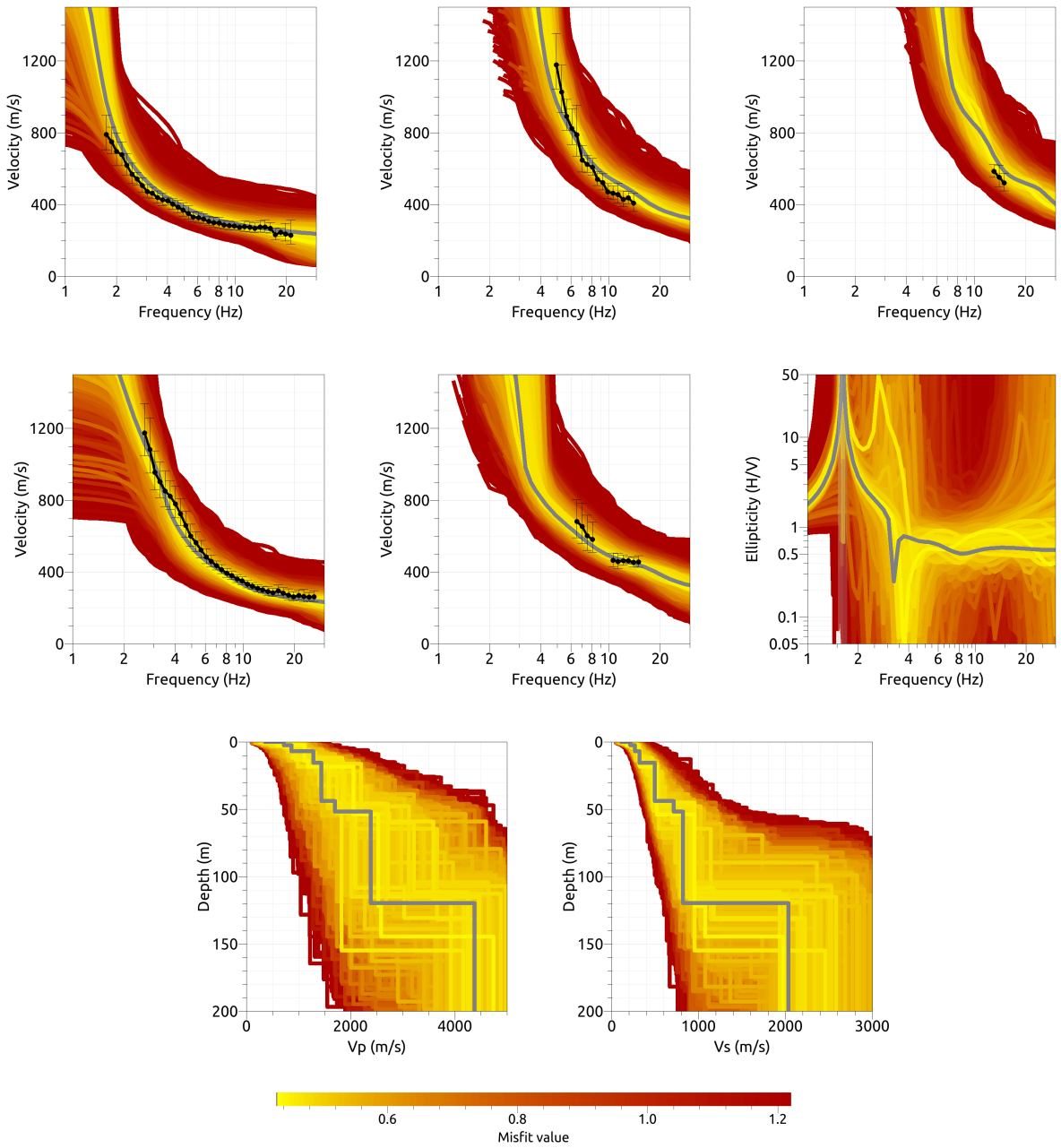

Figure 19: Inversion SVEJ8l. Top line: Dispersion curves for the Love wave fundamental mode (left), first harmonic mode (center) and second harmonic mode (right). Center line: Dispersion curves for the Rayleigh wave fundamental mode (left) and first harmonic mode (center), ellipticity curve of the Rayleigh wave fundamental mode (right). Bottom line: P-wave velocity profiles (left) and S-wave velocity profiles (right). The black dots indicate the data points used for the inversion, the gray line indicates the best-fitting model.

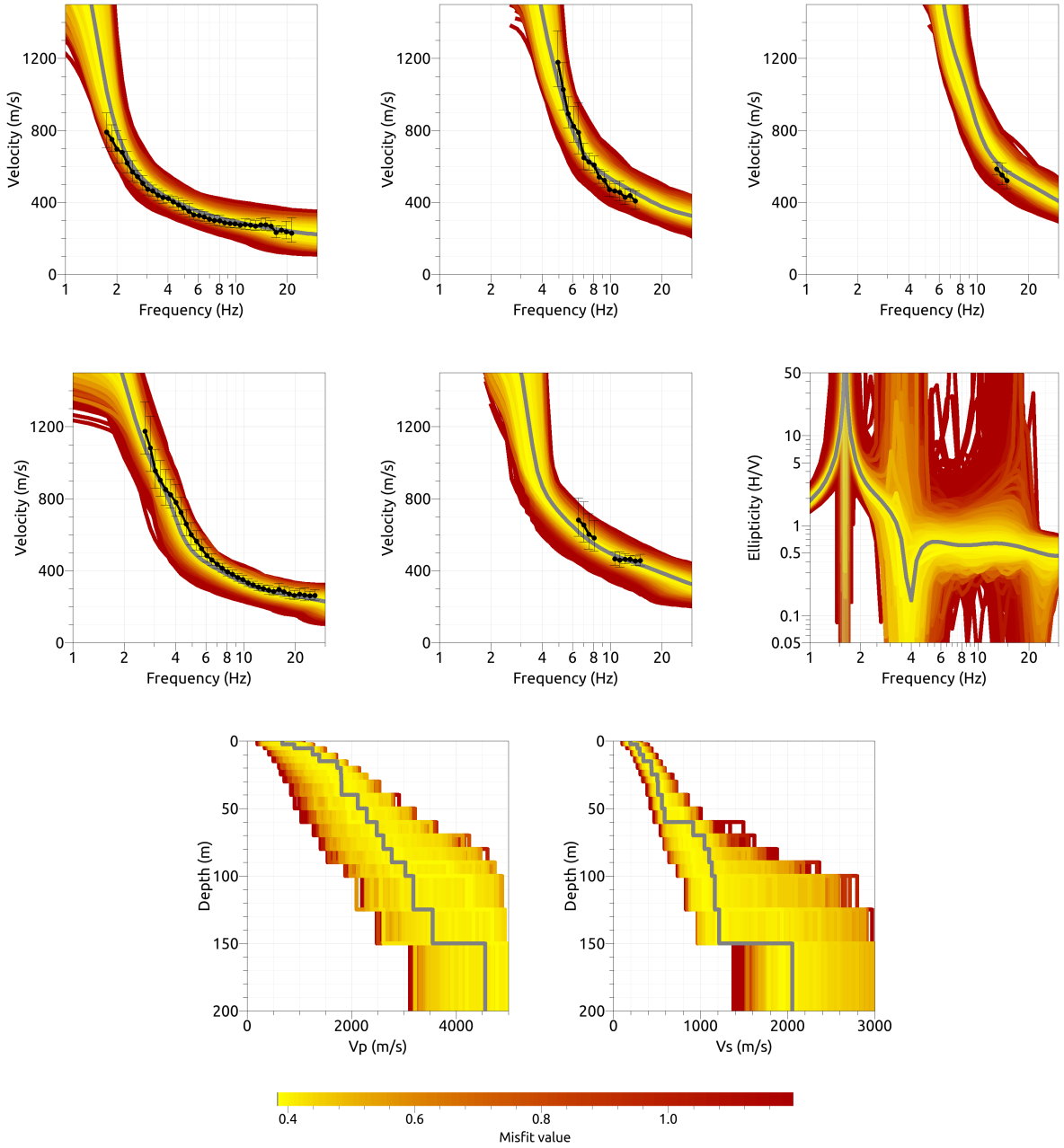

Figure 20: Inversion SVEJfix. Top line: Dispersion curves for the Love wave fundamental mode (left), first harmonic mode (center) and second harmonic mode (right). Center line: Dispersion curves for the Rayleigh wave fundamental mode (left) and first harmonic mode (center), ellipticity curve of the Rayleigh wave fundamental mode (right). Bottom line: P-wave velocity profiles (left) and S-wave velocity profiles (right). The black dots indicate the data points used for the inversion, the gray line indicates the best-fitting model.

5.4 Discussion of the inversion result

The best-fitting models of the inversions are shown in Fig. 21. All inversions give very similar profiles in the superficial 30 m, with a more or less smooth increase of the S-wave velocity from about 200 m/s at the surface to about 500 m/s. Below 30 m, the models differ more. Models with four to eight layers show velocity increases to 730 to 900 m/s in the depth range between 37 and 52 m/s and another strong velocity contrast between 100 and 150 m of depth. Below, the models find the seismic bedrock with S-wave velocities of around 2000 m/s. The three-layer model has less complexity and shows a first velocity contrast at 14 m depth (change from 270 to 530 m/s) and a second one at 75 m (increase to 2700 m/s). The inversion with fixed layer depths yields a model with mostly steady velocity increases, a first velocity contrast at 60 m depth and a second, more pronounced one at 150 m depth.
Overall, the models with four to eight layers are in good agreement with the fixed depth approach and the model with only three layers seems not complex enough to explain the data well enough. In the following, we use all inversions except the three-layer inversion as representative solutions.
The findings are in good agreeement with the geological profile information from the borehole about 260 m to the east of station SVEJ, where alluvial deposits range to a depth of 49.5 m, overlying the molasse. Therefore, we can interpret the velocity contrast found between 37 and 52 m as the contrast between the alluvia and the molasse.
The three-layer model has a V_{S30} of 368.6 m/s, all other inversions give models with V_{S30} between 348.0 and 354.9 m/s, with an average value of $351.2 \pm 2.7\, m/s$.

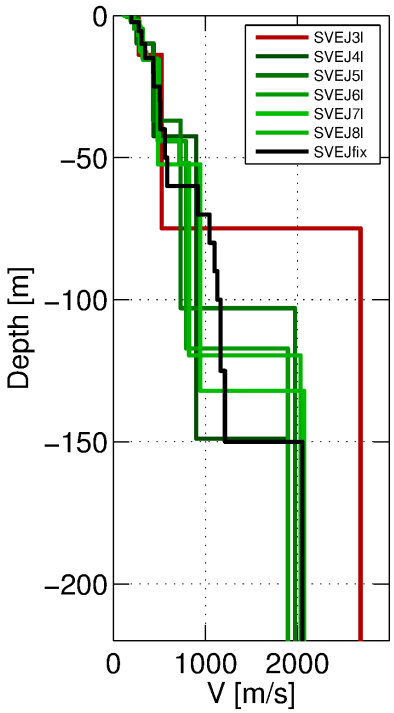

Figure 21: Overview of the shear-wave velocity profiles of the the different inversions.

5.5 SH transfer function

The empirical amplification for station SVEJ is based on only eight events so far and the statistical quality of the curve will certainly increase in the future. In Fig. 22, the theoretical shear-wave transfer functions for the inversion results are compared with the empirical amplification. Both curves are in good agreement around the fundamental peak, even if the empirical amplification has a fundamental frequency of 1.5 Hz and the inversion results at 1.62 Hz. The secondary peak around 3.75 Hz is also very similar in both curves and also in the higher frequency range, there is a good overall agreement.

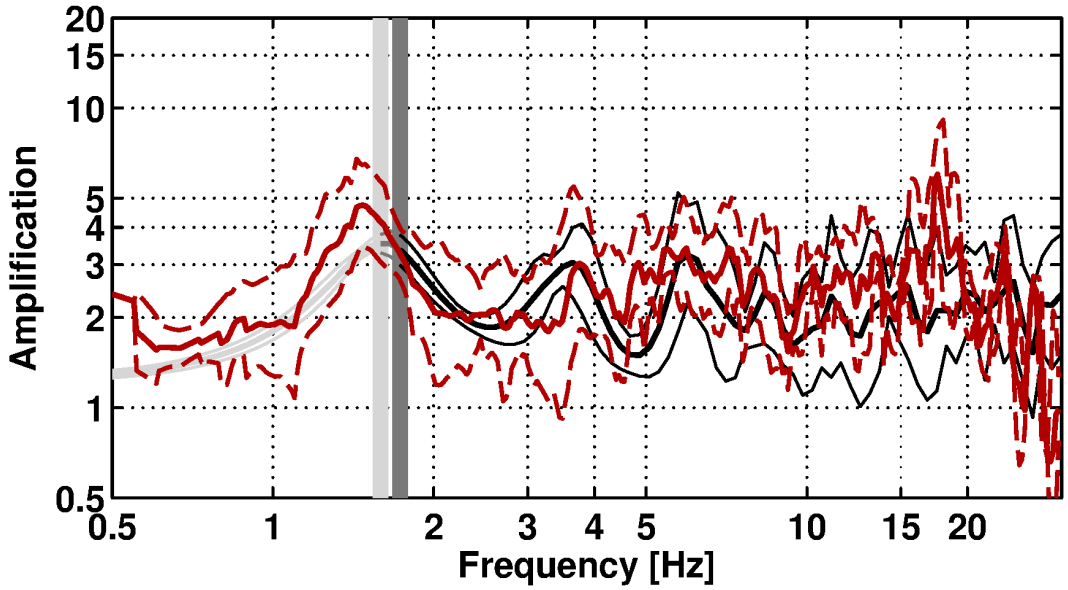

Figure 22: Comparison between the modeled amplification for the best models of the six inversions with at least four layers (black, with standard deviation) and the empirical amplification measured at station STHK (red, with standard deviation). The vertical light and dark grey bars correspond to the ellipticity peak frequency and the lowest frequency of the dispersion curves, respectively.

5.6 Quarter-wavelength representation

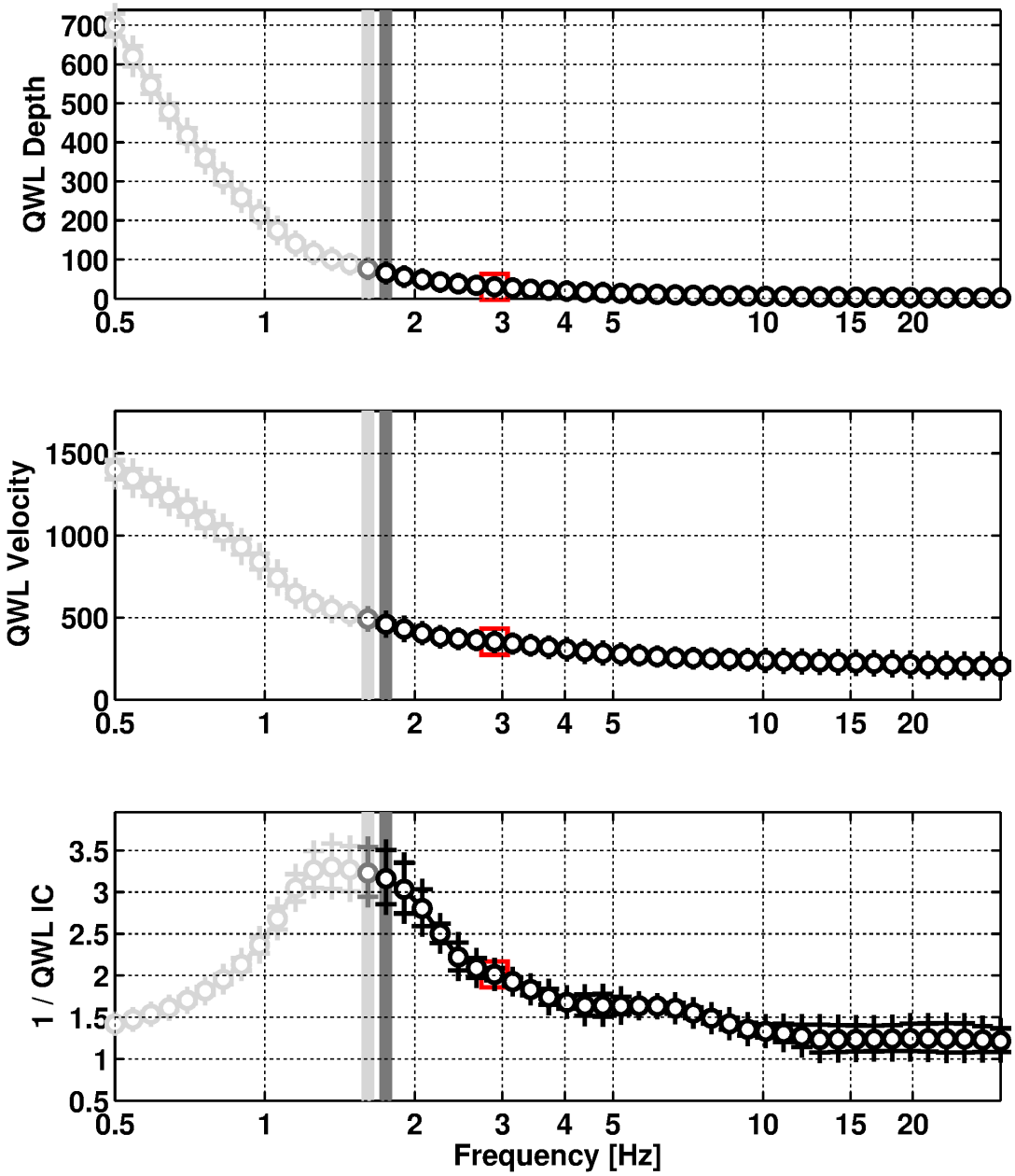

Figure 23: Quarter wavelength representation of the velocity profile for the best models of the inversions (top: depth, center: velocity, bottom: inverse of the impedance contrast). The black curves are constrained by the dispersion curves, the light grey curves are not constrained by the data. The red square corresponds to V_{S30}.

6 Conclusion

We performed a passive array measurement to characterize the soil underneath station SVEJ in Vevey (VD), located on an alluvial fan close to the lake shore of Lake Geneva. The dispersion curves for Love and Rayleigh waves could be measured over a wide frequency range. The Love wave dispersion curve was measured between 1.7 and 21.2 Hz (fundamental mode), also two higher modes could be identified. For the Rayleigh waves, the fundamental mode dispersion curve was retrieved between 2.6 and 26.1 Hz, and also a higher mode was identified. The H/V and ellipticity measurements of the different methods were not in good agreement and therefore not used in the inversion for the soil structure. Only the fundamental H/V peak frequency around 1.62 Hz was used for the inversion.
The joint inversion of Love and Rayleigh wave dispersion and ellipticity curves showed that the structure can be explained by models with at least four layers. In the superficial 30 m, the best models show a smooth increase of the S-wave velocity from 200 to 500 m/s. A first velocity contrast is found between 37 and 52 m, a second one with the bedrock between 100 and 150 m. The V_{S30} of the best models is about 351 m/s, corresponding to soil class C in both EC8 and SIA261.

Acknowledgements

The authors thank David Farsky and Simon Rouwendaal for their help during the array measurements.

References

Aki, K. (1957). Space and time spectra of stationary stochastic waves, with special reference to microtremors. *Bull. Earthquake Res. Inst. Tokyo Univ.*, 35:415–456.

Bettig, B., Bard, P.-Y., Scherbaum, F., Riepl, J., Cotton, F., Cornou, C., and Hatzfeld, D. (2001). Analysis of dense array noise measurements using the modified spatial auto-correlation method (SPAC): application to the Grenoble area. *Boll. Geof. Teor. Appl.*, 42:281–304.

Burjánek, J., Gassner-Stamm, G., Poggi, V., Moore, J. R., and Fäh, D. (2010). Ambient vibration analysis of an unstable mountain slope. *Geophys. J. Int.*, 180:820–828.

Burjánek, J., Moore, J. R., Molina, F. X. Y., and Fäh, D. (2012). Instrumental evidence of normal mode rock slope vibration. *Geophys. J. Int.*, 188:559–569.

Fäh, D., Wathelet, M., Kristekova, M., Havenith, H., Endrun, B., Stamm, G., Poggi, V., Burjanek, J., and Cornou, C. (2009). Using ellipticity information for site characterisation. NERIES deliverable JRA4 D4, available at http://www.neries-eu.org.

Hobiger, M., Bard, P.-Y., Cornou, C., and Le Bihan, N. (2009). Single station determination of Rayleigh wave ellipticity by using the random decrement technique (RayDec). *Geophys. Res. Lett.*, 36.

Maranò, S., Reller, C., Loeliger, H.-A., and Fäh, D. (2012). Seismic waves estimation and wavefield decomposition: Application to ambient vibrations. *Geophys. J. Int.*, 191:175–188.

Poggi, V. and Fäh, D. (2010). Estimating Rayleigh wave particle motion from three-component array analysis of ambient vibrations. *Geophys. J. Int.*, 180:251–267.